

# Nonradiative relaxation times in diagonal transition Si/SiGe quantum cascade structures

I. Bormann,<sup>a)</sup> K. Brunner, S. Hackenbuchner, and G. Abstreiter

Walter Schottky Institut, Technische Universität München, Am Coulombwall, D-85748 Garching, Germany

S. Schmult and W. Wegscheider

Institut für Angewandte und Experimentelle Physik, Universität Regensburg, D-93040 Regensburg, Germany

(Received 20 June 2003; accepted 8 October 2003)

Here, we explore experimentally and theoretically the possibility to prolong the upper hole state nonradiative lifetime of Si/SiGe quantum cascade (QC) structures by using a spatially indirect diagonal transition between two SiGe quantum well ground states. With the recent observation of well resolved midinfrared electroluminescence from heavy hole intersubband transitions in Si/SiGe valence-band QC structures, a Si-based QC laser seems no longer to be out of reach. A long carrier lifetime and maybe population inversion, however, appear to be impossible for structure designs with a vertical intersubband transition studied so far. This is due to the nonresonant behavior of deformation potential scattering dominant in unipolar SiGe. We report on calculations of the band structure using a six-band  $\mathbf{k}\cdot\mathbf{p}$  model and of hole deformation potential scattering that predict significantly increased nonradiative lifetimes for large barrier thickness, reaching about 20 ps for 35 Å Si barrier layer width. Electroluminescence measurements of a series of QC structures with varied barrier width reveal comparable efficiencies and the deduced lifetimes confirm our model calculations. © 2003 American Institute of Physics. [DOI: 10.1063/1.1631381]

Unipolar intersubband lasers like quantum cascade lasers (QCL) might be realized not only in III–V semiconductors but also in Si/SiGe structures. By using intersubband transitions within the same band, one can circumvent the main obstacle to silicon-based lasers, the indirect band gap. The large band offsets in the valence band of pseudomorphic SiGe layers on Si substrates imply a quantum cascade (QC) scheme with hole subbands. Midinfrared (MIR) electroluminescence (EL) from Si/SiGe-based QC structures has already been demonstrated.<sup>1,2</sup> However, no optical gain or stimulated emission has been demonstrated so far. In order to come closer to a silicon-based QC laser, a hole state QC structure that can achieve population inversion has to be designed. Thanks to the resonant behavior of the dominant Fröhlich interaction of electrons with optical phonons in polar semiconductors, a long (short) lifetime in the higher (lower) subband can be achieved simply by an adequate design of the subband energy spacings in present QCLs. In nonpolar semiconductors like Si and Ge, the dominant nonradiative scattering mechanism is deformation potential scattering that does not show such a resonant behavior. Calculations of Rimann *et al.*<sup>3</sup> have shown, that optical phonon scattering of holes monotonically increases with increasing subband spacing, if it is larger than the optical phonon frequencies, a situation required for MIR emission. A short lifetime of 0.25 ps was observed by recent fs MIR pump–probe studies of a vertical optical transition between two heavy hole subbands (HH2–HH1) in a Si/SiGe quantum well (QW).<sup>4</sup>

In this work, we investigate the possibility to achieve long hole lifetimes in diagonal radiative transition Si/SiGe QC structures. We present nonradiative lifetime calculations

within a  $\mathbf{k}\cdot\mathbf{p}$  model and EL measurements from cascade structures with diagonal transitions across barriers of varied width. The results are compared to that of a similar structure with vertical transition. The model calculations and the experimentally observed EL response are in good agreement.

The band structure of one period in a Si/SiGe QC structure with a diagonal optically active transition across a Si barrier layer is shown in Fig. 1. By varying the Si barrier layer thickness, the overlap of the wave functions of the HH2 and HH1 subbands and consequently the hole lifetimes can be tuned. The design of the QC structures is very similar to

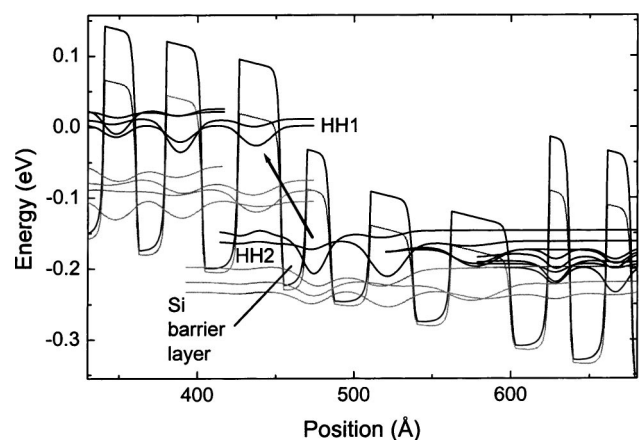


FIG. 1. Calculated subband structure of a diagonal transition Si/SiGe QC structure (with 15 Å Si barrier) grown pseudomorphically on Si: Potential for  $k_{\parallel}=0$  at an applied electric field of 55 kV/cm and squared envelope wave functions for heavy (black) and light holes (gray) calculated in an effective mass model. Layer thickness (in Å) and Ge content of the QW and Si barriers are from the right- to left-hand side: 18/0.43, 21/0, 16/0.43, 21/0, 41/0.24, 21/0, 30/0.24, 24/0, 17/0.29, 15/0, 28/0.43, 23/0, 24/0.43, 18/0, 21/0.43, 20/0. Underlined layers are  $p$ -doped with boron at  $1 \times 10^{18} \text{ cm}^{-3}$ . For the vertical radiative transition structure, the double QW structure (bold values) was replaced by a single QW (39 Å/0.39).

<sup>a)</sup>Author to whom correspondence should be addressed; electronic mail: ingo.bormann@wsi.tu-muenchen.de

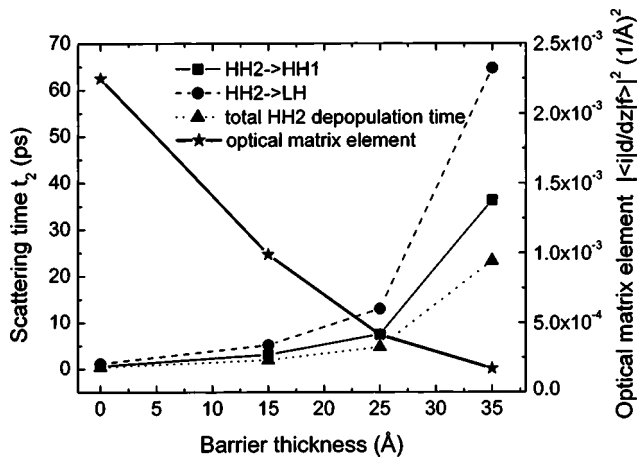


FIG. 2. Calculated nonradiative scattering times for the HH2→HH1 and HH2→LH transition and total depopulation time of the HH2 level vs barrier thickness. Stars show the corresponding calculated optical matrix element. The values for the vertical transition are plotted at barrier thickness zero.

the structures we studied earlier with exception of the diagonal transition scheme.<sup>2</sup> We investigate three pseudomorphic Si/SiGe QC structures on (001) Si with diagonal transitions across Si barriers of 15 Å, 25 Å, and 35 Å thickness and a vertical transition sample where the two QWs that feature the diagonal transition are replaced by one QW of 39 Å thickness and 39% Ge content. The structures are not designed to actually show population inversion or optical gain.

The structures make use of an EL transition between two heavy hole subbands HH2 and HH1 in neighboring QWs (Fig. 1). Holes are injected by tunneling through a HH miniband into the HH2 subband on the right-hand side of the active region. After a diagonal transition down into the lower HH1 subband, see arrow in Fig. 1, either by phonon scattering or MIR photon emission, holes are extracted by another HH miniband to the left-hand side out of the active region.

We have calculated the band structures within a six-band  $\mathbf{k}\cdot\mathbf{p}$  model using the parameters given in Ref. 5 and the Nextnano3D software package.<sup>6</sup> The calculation includes Ge segregation effects within a two-state exchange kinetic model using parameters from Ref. 7. From the resulting subband structure, we have calculated the optical matrix element  $\langle i|p_z|f\rangle$  at the  $\Gamma$ -point, where  $|i\rangle$  and  $|f\rangle$  denote the initial and final hole states and  $p_z$  is the momentum operator in the  $z$  direction, which is the direction perpendicular to the layers. Since we are only considering a transition between HH-like states, the matrix elements of  $p_x$  and  $p_y$  vanish. In addition, we have calculated the hole-phonon matrix element  $\langle i|D\cdot u|f\rangle$ , where  $D$  denotes the deformation potential tensor as described in Ref. 8. We assume a weighted alloy optical phonon spectrum consisting of Si-Si (64.3 meV), Si-Ge (50.8 meV), and Ge-Ge (37.4 meV) modes<sup>9</sup> for the atomic displacements  $u$ . By applying Fermi's golden rule and integrating over all final states, we obtain the scattering times.

In Fig. 2, the results of our calculations are depicted for varied Si barrier width. Phonon scattering of holes in a HH2 state takes place via two channels, scattering from the HH2 state into the HH1 subband or into the intermediate LH subband located between HH2 and HH1. As expected, the scattering times for both channels increase with increasing Si barrier width. This results in an increase of the calculated

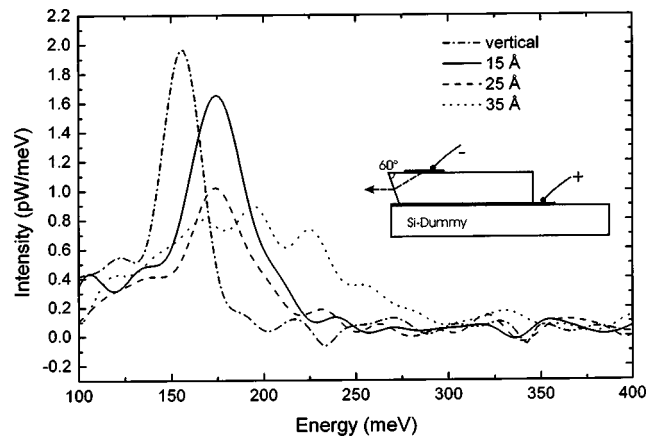


FIG. 3. Spectra of the four samples at 50 K and 450 mA driving current measured with 4  $\mu\text{s}$  pulse width and 10.7  $\mu\text{s}$  pulse period.

total HH2 nonradiative lifetime calculated by summing up the two channels from 1.9 ps for a 15 Å Si barrier layer up to 23 ps for 35 Å Si. According to Fermi's golden rule, the optical transition probability is proportional to  $|\langle i|p_z|f\rangle|^2$ . The squared matrix element (divided by  $\hbar^2$ ) drops from  $9.9\times 10^{-4} \text{ 1/\AA}^2$  (corresponding to a dipole moment  $|\langle i|z|f\rangle|$  of 6.2 Å) for 15 Å Si to  $1.7\times 10^{-4} \text{ 1/\AA}^2$  for 35 Å Si. For comparison, the vertical transition features a squared matrix element of  $2.25\times 10^{-3} \text{ 1/\AA}^2$  and a much smaller depopulation time of 0.4 ps. These results indicate that it should be possible to significantly increase the HH2 state lifetime by incorporating a barrier layer of adequate thickness, while still maintaining a reasonably high optical matrix element required for efficient EL emission or optical gain.

In order to experimentally verify the results of our calculations, we have fabricated four QC structures. The samples were grown by molecular-beam epitaxy on a  $2\times 10^{16} \text{ cm}^{-3}$   $p$ -doped (100) Si substrate at a substrate temperature of 430 °C. Each sample consists of a 400 nm thick  $6\times 10^{18} \text{ cm}^{-3}$   $p$ -doped Si layer, followed by ten QC periods and another 200 nm thick  $6\times 10^{18} \text{ cm}^{-3}$   $p$ -doped Si-layer. On top, there is a 30 nm Si layer  $p$  doped to  $1\times 10^{20} \text{ cm}^{-3}$ , for ohmic contacts. We have processed the samples into  $(410 \mu\text{m})^2$  mesas. A 60° facet close to the mesa is used to couple light out of the structure, see inset of Fig. 3. Evaporated Al/Au films on top of the mesas and on the wafer back side serve as contacts.

The structures were characterized by x-ray diffraction measurements. All samples are of high quality and show no signs of strain relaxation. The Ge content and QC period deviate slightly from the nominal values but they keep constant throughout the series of samples. This, together with the very good reproducibility of our boron doping, permits comparisons to be made within this sample series.

We used a Fourier transform infrared Nicolet spectrometer and a HgCdTe detector for recording the EL in a step scan lock-in technique. Mounted within a He-flow cryostat, two mesas were pumped in parallel in order to reach a higher detector signal level.

Figure 3 shows EL spectra from all structures at 50 K. The vertical transition structure reveals a distinct EL line centered at 155 meV, the diagonal transition structures with 15 Å and 25 Å Si barrier at 174 meV, and the 35 Å structure

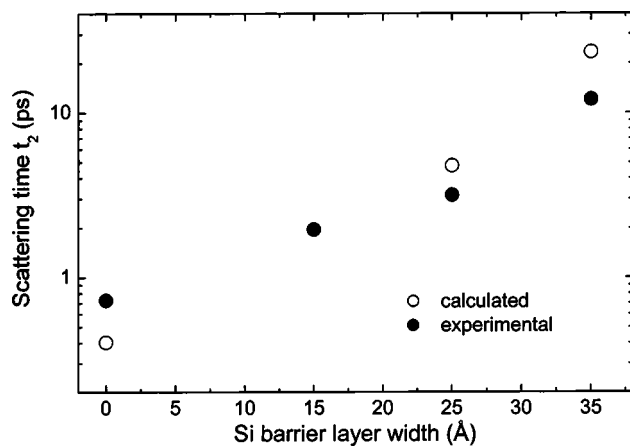


FIG. 4. Comparison of calculated and experimental nonradiative scattering times as derived from the EL intensity.

at 185 meV. The calculated emission energies are 136 meV, 149 meV, 155 meV, and 162 meV, respectively. The systematic deviation of experimental and calculated values is attributed to the slight difference of nominal and actual SiGe layer properties. The observed EL linewidth is smallest for the vertical transition (26 meV) and slightly larger (39 meV) for the 15 Å and 25 Å samples. This may be due to increased interface scattering or fluctuations in the thickness of the (upper state) QW. The HH2 subband energy is very sensitive to the SiGe QW thickness, due to its small value of 17 Å. There is no clear explanation for the much broader (about 100 meV) EL from the 35 Å sample. It may indicate the occupation of other excited hole subbands or of higher lying  $k_{\parallel}$  states within the in-plane dispersion of the HH2 level, caused by a very long nonradiative relaxation time and thermal heating of carriers. Further, inhomogeneous broadening due to an inhomogeneous field distribution within the periodic QC, as well as hot carrier effects, cannot be excluded. From bandstructure calculations, we expect a shift of the EL energy of only 0.33 meV cm/kV in the 15 Å case and 0.44 meV cm/kV in the 25 Å case, which is below our spectral resolution at such small intensities.

The optical matrix element enters quadratically into the radiative transition rate. Solving the simple rate equation for competing radiative and nonradiative relaxation channels of HH2 states, the spontaneous EL intensity is expected to be proportional to  $|\langle i|p_z|f\rangle|^2 \cdot t_2$ . In order to compare the measured EL to our model predictions, we have thus integrated the EL spectra getting the total EL intensity  $I$  at constant pump current and have deduced experimental nonradiative scattering times by  $t_2 = cI/|\langle i|p_z|f\rangle|^2$ . The constant  $c$  is an unknown factor, which is influenced by our experimental sensitivity and QC parameters like the injection efficiency into the HH2 subband. The thickness of the Si barrier has nearly no influence on the energetic position and shape of the HH2 wave function with respect to the adjacent injector subbands in the diagonal samples. There is also no difference in the current–voltage curves of the diagonal samples, with an onset of current flow at about 2 V. Therefore, the injection efficiencies should be similar, except maybe for the vertical transition sample. Thus, we assume  $c$  to be constant and calibrated it by setting the experimental and calculated scattering times equal for the 15 Å Si barrier structure. This

enables us to compare the variation of experimental and theoretical scattering times depending on Si layer width, see Fig. 4. The optical matrix element, that enters in the determination of the experimental scattering times, is simple to calculate from the band structure and it is, therefore, considered to be quite accurate. As predicted by the model calculations, the experimental scattering times show a strong increase with increasing barrier thickness and reach about 12 ps for the 35 Å barrier sample. The structure with vertical transition reveals a scattering time 0.7 ps compared to a calculated value of 0.4 ps. The calculated drastic change of the HH2 nonradiative lifetime by a factor of 60 is not fully verified by the experimental results revealing a factor of 17. The spectrally integrated intensity of the EL observed from the structures is nearly independent from the design of the optically active region (Fig. 2). The lack of an increase in EL intensity proposed by the calculations for large Si barrier width and HH2 lifetime may be due to additional hole scattering channels for those structures. We did not include interface scattering mechanisms and hole–hole scattering in our calculations. The latter cannot dissipate energy to the crystal lattice. Electron–electron scattering, however, was shown to be strong in recent terahertz devices and to alter the carrier energy distribution, resulting in modified optical phonon scattering rates.<sup>10</sup> Additionally, the HH2 states are only about 80 meV in energy below continuum states and may escape, especially when the upper state lifetime becomes long. Nevertheless, the large increase of HH2 scattering time deduced from EL measurements confirms the qualitative behavior predicted by the calculations. Nonradiative hole relaxation is strongly reduced in Si/SiGe hole QC structures with a diagonal transition across an adequate Si barrier layer.

In conclusion, scattering times determined from EL spectra are in good agreement with deformation potential phonon scattering calculations for hole subbands in QC structures with varied Si barrier width. Both reveal an increase of hole lifetime within the upper states of more than an order of magnitude for diagonal transitions across a 35 Å Si barrier layer compared to vertical transitions. Thus, diagonal transitions may enable population inversion of heavy hole subbands within a Si/SiGe QC structure for the price of a reduced optical matrix element.

This work was financially supported by the DFG (Br1960/1-3).

- <sup>1</sup>G. Dehlinger, L. Diehl, U. Genser, H. Sigg, J. Faist, K. Ensslin, D. Grützmacher, and E. Müller, *Science* **290**, 2277 (2000).
- <sup>2</sup>I. Bormann, K. Brunner, S. Hackenbuchner, G. Zandler, G. Abstreiter, S. Schmult, and W. Wegscheider, *Appl. Phys. Lett.* **80**, 2260 (2002).
- <sup>3</sup>K. Reimann, R. A. Kaindl, and M. Woerner, *Phys. Rev. B* **65**, 045302 (2001).
- <sup>4</sup>R. A. Kaindl, M. Wurm, K. Reimann, M. Woerner, T. Elsaesser, C. Miesner, K. Brunner, and G. Abstreiter, *Phys. Rev. Lett.* **86**, 1122 (2001).
- <sup>5</sup>M. M. Rieger and P. Vogl, *Phys. Rev. B* **48**, 14276 (1993).
- <sup>6</sup>M. Sabathil, S. Hackenbuchner, J. A. Majewski, G. Zandler, and P. Vogl, *J. Comput. Electron.* **1**, 81 (2002); <http://www.wsi.tu-muenchen.de/nextnano3/>
- <sup>7</sup>S. Fukatsu, K. Fujita, H. Yaguchi, Y. Shiraki, and R. Ito, *Appl. Phys. Lett.* **59**, 2103 (1991).
- <sup>8</sup>M. Woerner and T. Elsaesser, *Phys. Rev. B* **51**, 17490 (1995).
- <sup>9</sup>G. Sun and L. Friedman, *Phys. Rev. B* **53**, 3966 (1996).
- <sup>10</sup>R. Köhler, A. Tredicucci, F. Beltram, H. E. Beere, E. H. Linfield, A. G. Davies, D. A. Ritchie, R. C. Iotti, and F. Rossi, *Nature (London)* **417**, 156 (2002).